

PAPER • OPEN ACCESS

Minibeam radiotherapy with small animal irradiators; *in vitro* and *in vivo* feasibility studies

To cite this article: Soha Bazzyar *et al* 2017 *Phys. Med. Biol.* **62** 8924

View the [article online](#) for updates and enhancements.




Related content

- [Monte Carlo optimization of a microbeam collimator design for use on the small animal radiation research platform \(SARRP\)](#)
Nolan M Esplen, Lila Chergui, Chris D Johnstone *et al.*
- [Image-guided microbeam irradiation to brain tumour bearing mice using a carbon nanotube x-ray source array](#)
Lei Zhang, Hong Yuan, Laurel M Burk *et al.*
- [Evaluation of dose-volume metrics for microbeam radiation therapy dose distributions in head phantoms of various sizes using Monte Carlo simulations](#)
Danielle Anderson, E Albert Siegbahn, B Gino Fallone *et al.*

Recent citations

- [Monte Carlo optimization of a microbeam collimator design for use on the small animal radiation research platform \(SARRP\)](#)
Nolan M Esplen *et al*

Minibeam radiotherapy with small animal irradiators; *in vitro* and *in vivo* feasibility studies

Soha Bazyar^{1,7} , Christina R Inscoe^{2,3} , E Timothy O'Brian³,
Otto Zhou^{2,3,4} and Yueh Z Lee^{1,3,4,5,6,7} 

¹ Joint Department of Biomedical Engineering, The University of North Carolina at Chapel Hill and North Carolina State University, Chapel Hill, NC, United States of America

² Department of Applied Physical Sciences, The University of North Carolina at Chapel Hill, Chapel Hill, NC, United States of America

³ Department of Physics and Astronomy, The University of North Carolina at Chapel Hill, Chapel Hill, NC, United States of America

⁴ Lineberger Comprehensive Cancer Center, The University of North Carolina at Chapel Hill, Chapel Hill, NC, United States of America

⁵ Department of Radiology, The University of North Carolina at Chapel Hill, Chapel Hill, NC, United States of America

⁶ Biomedical Research Imaging Center, The University of North Carolina at Chapel Hill, Chapel Hill, NC, United States of America

E-mail: sbazyar@ncsu.edu and leey@med.unc.edu

Received 8 April 2017, revised 3 October 2017

Accepted for publication 10 October 2017

Published 10 November 2017



CrossMark

Abstract

Minibeam radiation therapy (MBRT) delivers an ultrahigh dose of x-ray (≥ 100 Gy) in 200–1000 μm beams (peaks), separated by wider non-irradiated regions (valleys) usually as a single temporal fraction. Preclinical studies performed at synchrotron facilities revealed that MBRT is able to ablate tumors while maintaining normal tissue integrity. The main purpose of the present study was to develop an efficient and accessible method to perform MBRT using a conventional x-ray irradiator. We then tested this new method both *in vitro* and *in vivo*. Using commercially available lead ribbon and polyethylene sheets, we constructed a collimator that converted the cone beam of an industrial irradiator to 44 identical beams (collimator size $\approx 4 \times 10$ cm).



Original content from this work may be used under the terms of the [Creative Commons Attribution 3.0 licence](https://creativecommons.org/licenses/by/3.0/). Any further distribution of this work must maintain attribution to the author(s) and the title of the work, journal citation and DOI.

⁷ Authors to whom any correspondence should be addressed.

The dosimetry characteristics of the generated beams were evaluated using two different radiochromic films (beam FWHM = $246 \pm 32 \mu\text{m}$; center-to-center = $926 \pm 23 \mu\text{m}$; peak-to-valley dose ratio = 24.35 ± 2.10 ; collimator relative output factor = 0.84 ± 0.04). Clonogenic assays demonstrated the ability of our method to induce radiobiological cell death in two radioresistant murine tumor cell lines (TRP = glioblastoma; B16-F10 = melanoma). A radiobiological equivalent dose (RBE) was calculated by evaluating the acute skin response to graded doses of MBRT and conventional radiotherapy (CRT). Normal mouse skin demonstrated resistance to doses up to 150 Gy on peak. MBRT significantly extended the survival of mice with flank melanoma tumors compared to CRT when RBE were applied (overall $p < 0.001$). Loss of spatial resolution deep in the tissue has been a major concern. The beams generated using our collimator maintained their resolution *in vivo* (mouse brain tissue) and up to 10 cm deep in the radiochromic film. In conclusion, the initial dosimetric, *in vitro* and *in vivo* evaluations confirmed the utility of this affordable and easy-to-replicate minibeam collimator for future preclinical studies.

Keywords: minibeam radiotherapy, radiotherapy, minibeam collimator, film dosimetry, spatial fractionated radiotherapy

 Supplementary material for this article is available [online](#)

(Some figures may appear in colour only in the online journal)

Introduction

Normal tissue toxicity is the dominant dose-limiting side effect of radiotherapy (RT) (Hendry *et al* 2006). Applying therapeutic doses of ionizing radiation to radiosensitive tissues such as in the brain almost always produces a certain level of radiation side effect. This effect not only occurs after conventional RT (CRT), but also following intensity-modulated radiotherapy (IMRT) and proton therapy (Armoogum and Thorp 2015). In contrast, spatially fractionated methods of RT have shown an increased preservation of healthy tissue (Dilmanian *et al* 2003, Dilmanian *et al* 2007, Yuan *et al* 2015, Nolan *et al* 2017). Relative to the homogeneous dose delivery in CRT, spatially fractionated modalities apply physically separated doses of radiation to the target. Of the types of spatially fractionated techniques, microbeam radiotherapy (MRT), which delivers quasi-parallel lines, less than $100 \mu\text{m}$ wide, of a single high dose (hundreds Gys) of irradiation (peaks), separated by wider non-irradiated regions (valleys), is a promising new approach (figure 1). Preclinical studies have consistently demonstrated the selective tumoricidal and normal tissue sparing effects of this method (Bouchet *et al* 2016, Smyth *et al* 2016). This suggests that a potential advantage of MRT is not only reduced radiation-related normal tissue toxicity, but also improved tumor control rates. This property would be of special benefit to pediatric and previously irradiated recurrent tumor patients, where radiation dose considerations are paramount. Ultra-high intensity parallel x-ray photons produced by synchrotron sources have the ideal characteristics for generating thousands Gys micro-beams. Unfortunately, such synchrotron sources are rare. At present, only three active synchrotron facilities in the world are running preclinical MRT studies. Aside from the difficulty in accessing these facilities, there is also a lack of specialized hospitals near them. Thus, MRT has not yet been clinically applied, mainly due to a lack of sufficient preclinical data.

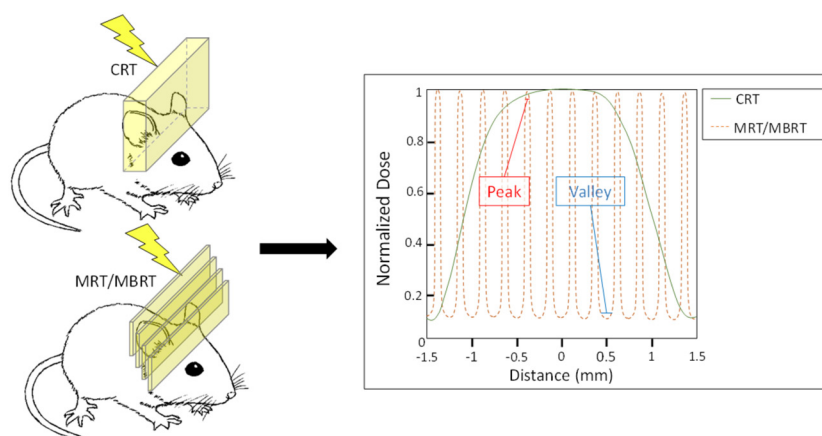


Figure 1. Schematic picture of conventional radiation therapy (CRT) versus spatially fractionated microbeam/minibeam radiation therapy (MRT/MBRT). In CRT, a homogeneous single dose of irradiation is delivered to the target (top mouse and continuous line in the graph), while in MRT/MBRT, a single high dose of irradiation deposits in micrometer beams (peak) that are separated by non-irradiated regions (valley) (bottom mouse and dashed line in the graph).

Recently, there have been some efforts to apply this promising method using non-synchrotron irradiators (Hong *et al* 2015, Bartzsch *et al* 2016). Nevertheless, the radiation profiles of these approaches suffered from the non-uniformity of the beams and valleys, and also the variability of the peak-to-valley dose ratios (PVDR). These are the critical parameters in the normal tissue sparing and therapeutic efficacy of the MRT (Bouchet *et al* 2016). In addition, there are multiple clinical limitations for microbeams as described before by Dilmanian *et al*, namely, loss of beam spatial resolution *in vivo* as a result of cardiorespiratory induced motion in the target organs (Dilmanian *et al* 2006). Therefore, slightly wider ‘minibeams’ ($200 \mu\text{m} \leq \text{FWHM} < 1 \text{ mm}$) have been proposed as a promising clinical future for this technique. Synchrotron-generated minibeams have also exhibited a normal tissue sparing effect for beams up to 0.68 mm in FWHM (Dilmanian *et al* 2006, Prezado *et al* 2015, Deman *et al* 2012). Babcock *et al* designed a collimator to mount near an industrial source to create minibeams (Babcock *et al* 2011). Although their method demonstrated the feasibility of utilizing a conventional x-ray tube to implement MBRT, their resultant beams were 1 mm wide. A recent study by Brönnimann *et al* revealed that beams $\geq 400 \mu\text{m}$ may induce an unfavorable microvascular response in normal tissue (Brönnimann *et al* 2016).

Our group developed the first desktop device for applying $300 \mu\text{m}$ wide beams using a multi-beam source, based on a field emission carbon-nanotube x-ray tube (Hadsell *et al* 2013). Our first-generation device was able to apply an image-guided, physiologically gated beam with an entrance dose rate of 21.7 mGy s^{-1} , and in a long run behavioral study, we found that the generated beams using our device were able to spare normal mouse brain tissue (Chitchevov *et al* 2014, Zhang *et al* 2014, Bazyar *et al* 2017). Since our first-generation device was not ready to generate an ultrahigh dose of hundreds Gy used in MBRT studies in a reasonable time frame, we sought to investigate the possibility of applying MBRT using a conventional irradiator and a simple and inexpensive collimator, to facilitate preclinical studies on MBRT. We found that this collimator can convert the cone beam of a small animal irradiator to 44 identical beams (collimator size $\approx 4 \text{ cm} \times 10 \text{ cm}$). The dosimetry characteristics of the generated beams were investigated by the simultaneous use of two radiochromic films with

Table 1. Comparison of XRAD-320 versus Xstrahl-300.

	XRAD-320 (preclinical)	Xstrahl-300 (Xstrahl Ltd, UK) (Clinical) ^a
Target material	Tungsten	Tungsten
Theta (degree)	30	30
Fixed filter	Br = 2 mm	Br = 0.8 ± 0.1 mm
Focal spot (largest diameter; mm)	8	≈7.5
Cooling system	Oil	Water to air; Water-cooled
Tube power max (kW)	4	3
Dose rate (Gy min ⁻¹)	2.9	2.16 (FSD = 20 cm; 150 kVp; filters = 2.25 mm Al and 0.15 mm Cu; mean energy = 62 KeV)
Dose measurement	PTW 7862 transmission chamber	N/A
1st HVL _{Al} (mm)	7.99 ± 0.41	

^a Data adopted from Xstrahl 200 and 300 (Xstrahl 200 and 300 2017).

different dose sensitivity ranges. Clonogenic assays revealed the induction of radiobiological cell death in two murine cell lines and initial *in vivo* studies demonstrated normal tissue sparing and the therapeutic advantage of our method relative to CRT. Although the loss of beam spatial resolution deep in the tissue is one of the major concerns in utilizing divergent industrial irradiators produced photons, the beams generated using our collimator kept their resolution *in vivo* and up to 10 cm deep in the radiochromic film. Here we demonstrate the properties of the collimator and the effectiveness of the device both *in vitro* and *in vivo* animal studies.

Materials and methods

Irradiation

An industrial small animal irradiator (X-RAD 320, PXi, North Branford, CT) was utilized as our radiation source. The tube specifications are presented in table 1 and compared to a clinical orthovoltage tube. This irradiator incorporates an oil-cooled anode, which enables running the device for multiple hours to generate hundreds Gy doses for the MBRT peaks. It also has an integrated plane parallel transmission chamber (PTW 7862, PTW, Freiburg, Germany), which can be cross-calibrated to an ionization chamber (we used MDH 1015, Radcal, Monrovia, CA; the sensitive area of detector ≈ 1 cm × 2m) at the desired focus-surface distance (FSD), to measure the dose rate and the total dose on-time. For all experiments, the tube was driven at 160 kVp and 25 mA to match our prior setting (Hadsell *et al* 2013). The beam was filtered with an additional 2 mm Al and the target was placed at 37 cm FSD.

Collimation

The minibeam were produced by a custom multi-slit collimator placed in close contact with the target (proximal collimation). The collimator consists of 5 mm thick lead ribbons, which block 99.999% of the primary photons in the highest energy spectrum range. To develop the collimator, a 0.6 mm thick, 5 mm wide lead ribbon was cut into 10 cm long pieces. A sandwich of 46 lead pieces was made by alternating 300 μm thick polyethylene sheets as spacers (figure 2(B)). The resulting collimator was 4 cm wide and 10 cm long (figure 2(A)).

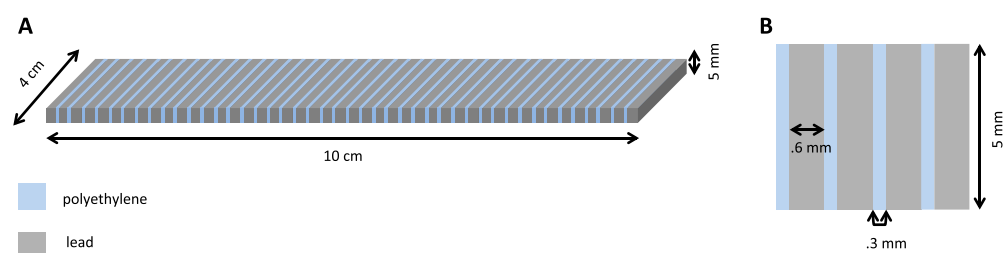


Figure 2. Minibeam collimator (A) top view of the collimator; (B) detailed layers of the collimator (the pictures are not drawn to the scale).

Dosimetry

SpekCalc version Pro was used to simulate the x-ray spectra (Poludniowski 2007, Poludniowski and Evans 2007, Poludniowski *et al* 2009). GAFCHROMIC™ MD-V3 (peak) and EBT3 (valley) films (Ashland Advanced Materials, Bridgewater, NJ, US) were utilized for dosimetry and evaluating dose profiles. The key technical features of GAFCHROMIC™ films that make them suitable for this purpose include the minimal response difference over a wide photon energy range, and high spatial resolution ($25\ \mu\text{m}$ or higher) (GAFCHROMIC™ Dosimetry Media, Type EBT-3; G GAFCHROMIC® MD-V2 Dosimetry Film). Consequently, several MRT and MBRT studies have used them for dosimetry evaluations (Crosbie *et al* 2008, Anderson *et al* 2010, Hadsell *et al* 2013b, Hong *et al* 2015). The films were cross-calibrated to the integrated plane parallel transmission chamber without any collimator in place and scanned 24 h later with 1200 dpi resolution (spatial resolution $\approx 20\ \mu\text{m}$) as previously described (Hadsell 2013a, Zhang *et al* 2014b). The scanned films were processed by a Matlab script (R-2015a, The MathWorks, Inc, Natick, MA) written in-house, using three-channel dosimetry principles described by Casanova Borca *et al* and the supplier (Casanova Borca *et al* 2013; Efficient Protocols for Accurate Radiochromic Film Calibration and Dosimetry 2017; GAFCHROMIC™ Dosimetry Tools 2017). Exposure doses were chosen such that peak and valley doses fell into the films' optimal sensitive range (1–10 Gy for EBT3 and 1–100 Gy for MD-V3) (GAFCHROMIC™ Dosimetry Media, Type EBT-3 2017; G GAFCHROMIC™ MD-V2 Dosimetry Film 2017).

A custom dose phantom was also created to evaluate the dose depth effects of the system. Ten layers of $4\text{ cm} \times 4\text{ cm}$ PMMA, with a thickness of 2 mm each, were sandwiched with 11 layers of GAFCHROMIC™ films of the same area to construct a phantom, as shown in the supplementary data figure 1 (stacks.iop.org/PMB/62/8924/mmedia). Data from this phantom were used to calculate the percentage dose drop (PDD) with and without the collimator, peak-to-valley-dose ratio (PVDR) and beam-width (full width half maximum = FWHM) of beams generated using the collimator. Since kilovolt energy photons were used in our experiments, the reference point (MU) was defined at the phantom surface. The field size ($4\text{ cm} \times 4\text{ cm}$) was matched to the clinical orthovoltage irradiator applicator at FSD = 30 cm (Xstrahl 200 and 300 2017). The aluminum first half-value-layer (HVL_{Al}) was evaluated following AAPM's TG-61 for kilovoltage x-ray beam dosimetry protocol setup (table 1 and supplemental figure 2(d)) (Ma *et al* 2001). All the experiments were repeated at least three times.

Cell culture and in vitro feasibility

A murine model of melanoma, B16-F10 cell line, was provided by the Lineberger Comprehensive Cancer Center Tissue Culture Facility, at the University of North Carolina at

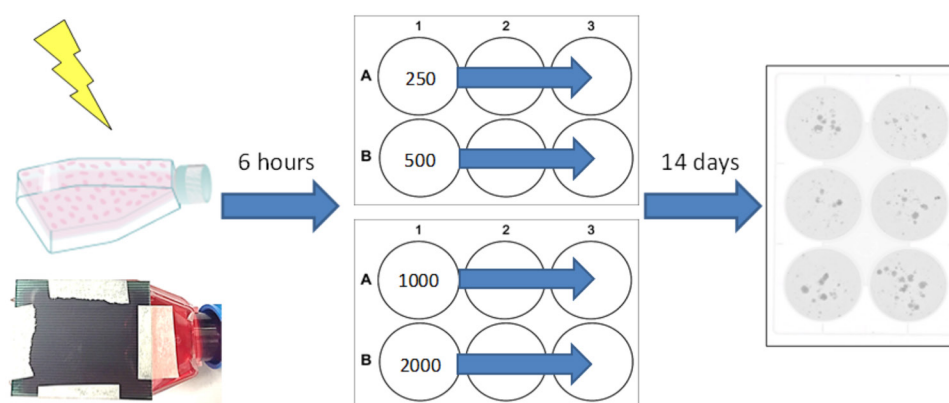


Figure 3. Schematic picture of the clonogenic assay protocol to investigate the *in vitro* effect of MBRT on two murine cancer cell lines (B16-F10 and TRP). Left bottom, is a picture of the irradiated cell culture flask with the attached radiochromic film on the top.

Chapel Hill (UNC-CH). A mouse model of glioblastoma, TRP cell line, was provided by Dr C Ryan Miller at UNC-CH (Schmid *et al* 2016). Cells were cultured at 37 °C and 5% CO₂ in Dulbecco's Modified Eagle's Medium supplemented with 10% FBS, 100 U ml⁻¹ penicillin and 100 µg ml⁻¹ streptomycin all from Corning Inc. (Corning, NY).

In vitro dose responses of B16-F10 and TRP cell lines were evaluated using clonogenic assays with delayed plating after treatment protocol as shown in figure 3 (Franken *et al* 2006). In short, an appropriate number of cells were seeded in 12.5 mm² cell culture flasks, grown to ≈90% confluency, and irradiated with different doses of MBRT. The flasks were filled with the complete media and placed upside down so that the collimator could be placed in close contact with the growth surface. To mimic the subcutaneous tumor dose, a 2 mm thick PMMA sheet was placed between the flask and the collimator. The control flasks were placed outside of the incubator inverted for an equal duration of time, to account for the effect of cell death due to detachment (anoikis) or an unfavorable environment (low temperature, humidity and pH). Six hours following irradiation, a single cell suspension was obtained and an appropriate number of cells was counted and seeded in each well of a 6-well plate. Colonies were fixed with 70% ethanol and stained with crystal violet two weeks later. After scanning, the colonies were counted using ImageJ (NIH, Bethesda, MD). The minimal pixel size of the particles was defined by measuring the size of a colony consisting of 25 cells for each cell line. The surviving fraction was calculated by the following equation:

$$\text{Plating efficiency (PE)} = \frac{\text{Number of Counted Colony}}{\text{Number of Platted Cells}} \times 100$$

$$\text{Surviving fraction (SF)} = \frac{\text{Irradiated Sample PE}}{\text{Control Sample PE}}.$$

In vivo feasibility

Five-week old female C57BL/6J mice were acquired from Jackson Laboratory (Bar Harbor, ME) and allowed to acclimate for a week before study initiation. The mice were housed in the UNC-CH Division of Laboratory Animal Medicine pathogen free designated environment and cared for in accordance with the United States Department of Health and Human

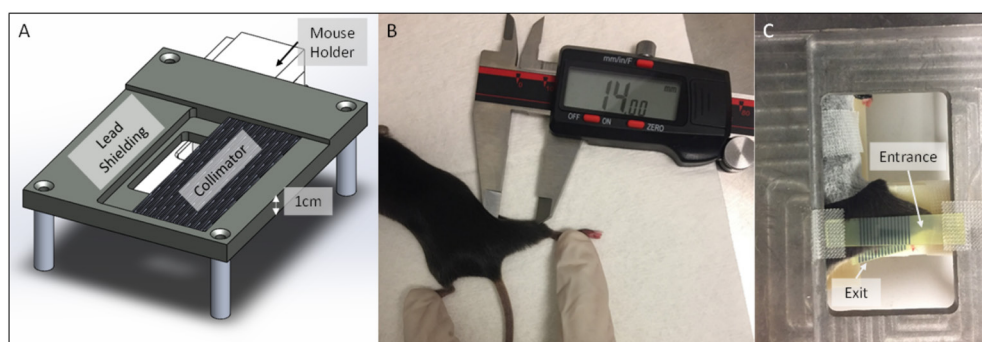


Figure 4. The *in vivo* studies setting. For all experiments, the anesthetized mouse was fixed on an in-house mouse holder and all of the body (except the irradiation field) was covered with 1 cm of lead. (A) CAD drawing of the irradiation setting. Note that the collimator is not shown all the way to the left to enable one to see the underneath shielding and mouse holder; (B) the radiation field was $1.5\text{ cm} \times 1.5\text{ cm}$ to cover the entire mouse thigh; (C) two pieces of Gafchromic[®] MD-V2 films were placed at the entrance and exit plans for dosimetry purposes.

Services Guide for the Care and Use of Laboratory Animals; all procedures were approved by UNC-CH Institutional Animal Care and Use Committee.

The mice underwent irradiation under anesthesia with 1%–2.5% isoflurane in medical-grade oxygen at a flow rate of $0.8\text{--}1\text{ L min}^{-1}$. Except for the irradiation field, the rest of the animal body was shielded with 1 cm thick lead (figure 4). The anesthetized mice were laid prone on an in-house designed mouse-holder and the head was fixed using ear bars and nose cone and their right thigh was fixed on the designated holder using medical tape.

To evaluate the effect of our method on normal skin, the right hind limbs of mice were shaved and irradiated with graded doses of CRT or MBRT (5 mice per group) and observed three times a week for the appearance of acute skin effect up to one month post-irradiation. The contralateral legs served as the control. Upon appearance, the skin effect was scored based on scoring system, illustrated in table 2 (Pommier *et al* 2004).

To investigate the spatial resolution of the beam *in vivo*, the mid and posterior part of a mouse brain was irradiated using the collimator with 100 Gy beams. Brain tissue from the animal was collected 6 h post-irradiation.

The mouse model of melanoma was prepared by subcutaneous injection of 1×10^5 B16-F10 cells in the right hind limb of the mice. The cells were prepared and injected based on the Overwijk *et al* protocol (Overwijk and Restifo 2001). One week later, mice were randomly assigned to three groups, and mice in CRT and MBRT groups received radiation on the inoculation site (MBRT = 150 Gy on peaks, CRT = 15 Gy). The tumor diameters were measured every other day and tumor volume was calculated using the formula $L \times W^2 \times 0.52$, where L is the longest dimension and W is the perpendicular dimension in mm. The mice were humanely sacrificed when the tumor burden reached the protocol specified volume of 1.2 cm^3 . The data was analyzed by SPSS (Ver. 22, IBM Corp., Armonk, NY). The P -value was calculated using a log-rank test.

Immunohistochemistry

A whole mouse brain was fixed in formalin for 48 h, processed, embedded in paraffin and serially sectioned at $5\ \mu\text{m}$ thickness. Sectioned slides were used for γ -H2AX

Table 2. Radiation therapy oncology group scoring system for acute radiation skin injury.

Score	0	1	2	3	4
Observation	No change over baseline	Erythema; dry desquamation; epilation	Bright erythema; moist desquamation; edema	Confluent moist desquamation; pitting edema	Ulceration, hemorrhage, necrosis

(Double-DNA-Strand-Break marker) immunofluorescence (IF) staining immediately. If staining was not done immediately, the unstained slides were stored in a nitrogen gas chamber. A rabbit monoclonal anti-phospho-ser 139-H2AX antibody was obtained from Cell Signaling Technology (Cat# 9718, Danvers, MA). IF was carried in the Bond Autostainer (Leica Microsystems Inc., Norwell, MA). All solutions were from Leica Microsystems (Norwell, MA). Slides were deparaffinized in Bond dewax solution (AR9222) and hydrated in Bond wash solution (AR9590), antigen retrieval of γ -H2AX was performed for 20 min at 100 °C in Bond-epitope retrieval solution 1 pH-6.0 (AR9961), then a protein blocking reagent (PV6122, Leica) was added for 10 min. After pretreatment, the slides were incubated for 2 h with γ -H2AX (1:2000). Detection was performed using the BondT Polymer Refine Detection system (DS9800) and Tyramide-Cy5 reagent (Perkin Elmer, SAT705A001EA). Slides were counterstained with Hoechst 33258 (H3569, Invitrogen, Carlsbad, CA) and mounted with a ProLong Gold antifade reagent (P36934, Life Technologies). Positive and negative controls (no primary antibody) were included. High-resolution acquisitions of IF slides in the DAPI and Cy5 channels were performed in the Aperio ScanScope FL (Leica) using 20 \times objective. Nuclei were visualized in a DAPI channel (blue) and γ -H2AX in Cy5 (red).

Results

At a FSD of 37 cm, XRAD 320 produced a homogenous 14.5 cm \times 14.5 cm radiation field (data not shown). The mean dose rate in the air at this distance was ≈ 2.9 Gy min⁻¹ (4.8 cGy s⁻¹) after the filters described in the table 1 (supplemental figures 2(a) and (b)). The simulated x-ray spectrum of the device can be found in the supplemental figure 1(c). The mean energy of the x-ray spectrum was 61 KeV and the 1st HVL_{A1} is 7.99 ± 0.41 (supplemental figure 1(d)). The mounted transmission chamber measured the dose within 1.25 ± 0.08 percentage difference compared to the cylindrical ion chamber.

The dosimetric characteristics of the collimator are shown in table 3.

The collimator (figure 2) was able to convert the cone beam of this irradiator to 44 mini-beams. The generated beam profile is shown in figure 5. In the *y*-direction (parallel to the beams), the peak did not decrease as the distance to the central axis increased (figure 5(B)). As shown in figure 5(C), the profile was uniform in the *x*-direction, and homogenous valleys were generated.

To study the behavior of the minibeams deep in the tissue, we measured the PDD of peak, valley and integral dose and PVDR at different depths using the PMMA phantom, and compared it with CRT (see supplemental figure 1 for detailed phantom measurements and setting). The results are shown in figure 6. It should be noted that the thickness of the radiochromic films (EBT3 = 278 μ m; MD-V3 = 255 μ m) were added to the PMMA sheet thickness (2 mm) to measure the depth of each point in the phantom. The entire doses in figure 6(A) were normalized to the mean entrance dose in CRT and the mean entrance integral dose in MBRT. Interestingly, the CRT and MBRT integral dose demonstrated a similar pattern in depth. The peak dose dropped to its half value at 19.61 ± 0.04 mm depth, while the valley

Table 3. Collimator dosimetric characteristics.

Beam FWHM (μm)	246 ± 32
Center-to-center (μm)	926 ± 23
Peak-to-valley dose ratio	24.35 ± 2.10
Relative output factor	0.84 ± 0.04

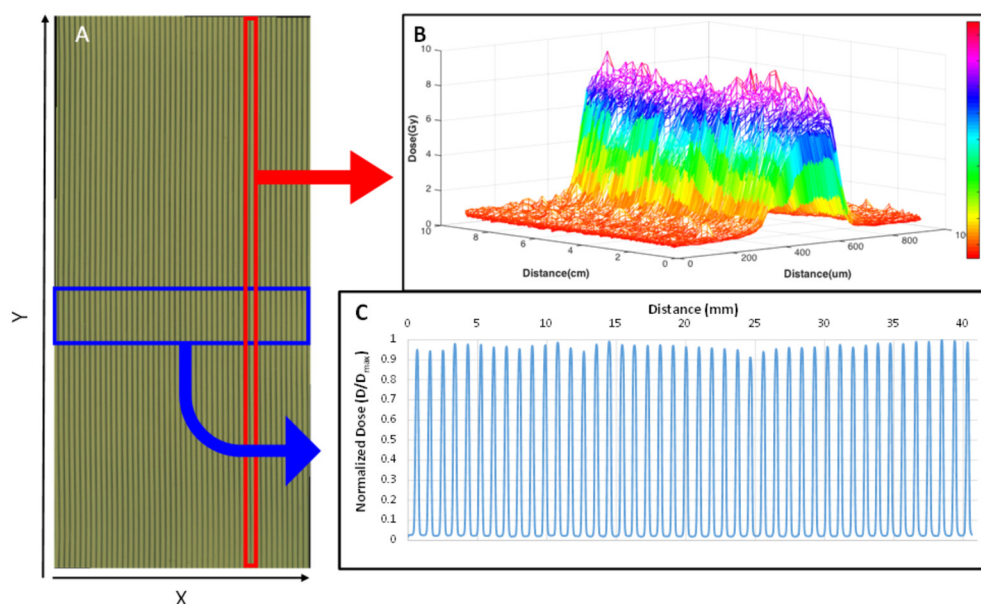


Figure 5. The beam profile at the PMMA phantom entrance (A) Gafchromic film showing the beam pattern. (B) A single beam pattern at the y -direction: the peak dose did not fall when the distance to the central axis increased. (C) The normalized beam profile in the x -direction: homogeneous peaks and valleys.

dose increased in the first 12.7 mm and then started to decrease. As a result of peak and valley dose behavior in the tissue, PVDR decreased exponentially and reached a plateau at a depth of almost 23 mm (figure 6(B)).

To investigate the cell response to the MBRT, the surviving fractions of the two cell lines after different doses of MBRT were calculated (figure 7).

One major concern in using non-synchrotron irradiators (divergent photons) to apply MBRT is the loss of spatial resolution deep in the tissue, as well as the potential formation of a homogeneous high dose radiation field that may cause tissue damage at the exit plane. The beam profile dependence on the depth of PMMA is shown in figure 6(C). The beams maintained their resolution at least up to the depth of our phantom (≈ 2.53 cm), sufficient for small animal studies, where the thickest portion of the body (head) in the prone position is around 2 cm. To further investigate the depth dependence of the beam, a $4\text{ cm} \times 10\text{ cm}$ EBT3 film was placed along the beam path (the longest dimension was parallel to the beams) between two 2 mm thick PMMA sheets and irradiated with 25 Gy (figures 8(A) and (B)). Interestingly, the peaks and valleys were distinguishable at a depth of 10 cm (figure 8(C)). To evaluate the spatial resolution of the beams *in vivo*, a mouse brain was irradiated with 100 Gy minibeam. The mouse was sacrificed 6 h post-irradiation and its brain tissue was stained with $\gamma\text{-H2AX}$,

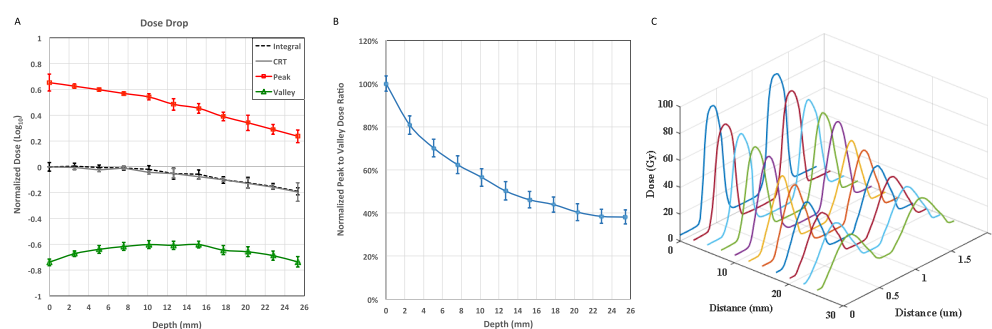


Figure 6. The dosimetric characteristics of minibeam at different depths of PMMA phantom. (A) PDD of peak, valley and integral dose versus CRT; please note that all the dose values were normalized to the entrance dose in CRT and the integral dose at the entrance plan in MBRT. (B) Percentage dose drop of the PVDR at different depths, normalized to the entrance PVDR. (C) The beam pattern at a different depth.

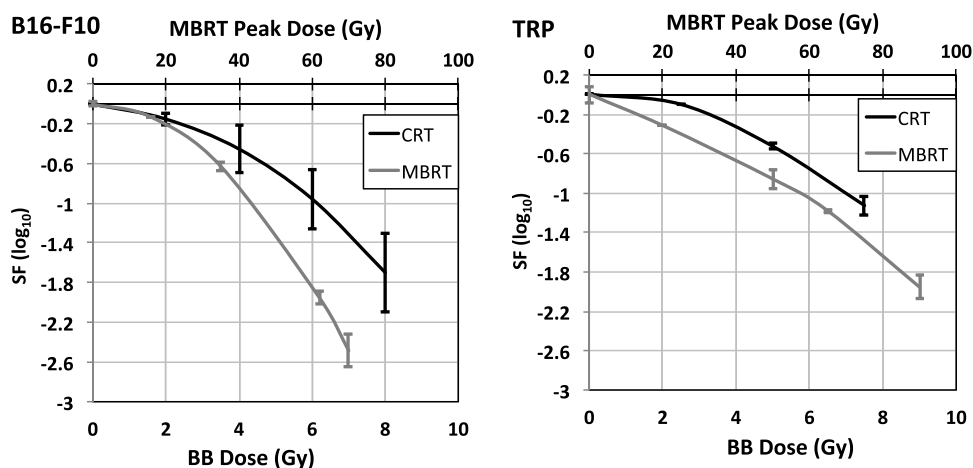


Figure 7. Cell survival curves. Surviving fraction versus the CRT dose and the MBRT peak dose of two different murine cell lines (B16-F10 on the right and TRP on the left), evaluated using the clonogenic assay. The CRT data are adopted from Twyman-Saint *et al* and Schmid *et al* for the B16-F10 and TRP cell line, respectively (Twyman-Saint *et al* 2015, Schmid *et al* 2016).

a DNA double-strand break marker. The mini-beams maintained their spatial resolution *in vivo* where physiological movements (heartbeat and respiration) were two major confounding factors (figure 8(D)).

To investigate the effect of MBRT on normal tissue and compare it with CRT, the right legs of normal mice were irradiated with graded doses of either irradiation modality (MBRT and CRT) and screened for the appearance of acute-skin effects (see table 2 for scoring detail). We observed that the highest doses that did not induce radiation side-effects in mice were 150 Gy and 15 Gy in MBRT and CRT, respectively (figure 9).

The therapeutic effect of our method was investigated by irradiating the mouse models of melanoma one week after right thigh inoculation. Using the current setting and the doses we applied, we found that tumor started to grow at a slower pace in MBRT and the mice in the MBRT group survived significantly longer than the other two groups ($p < 0.001$).

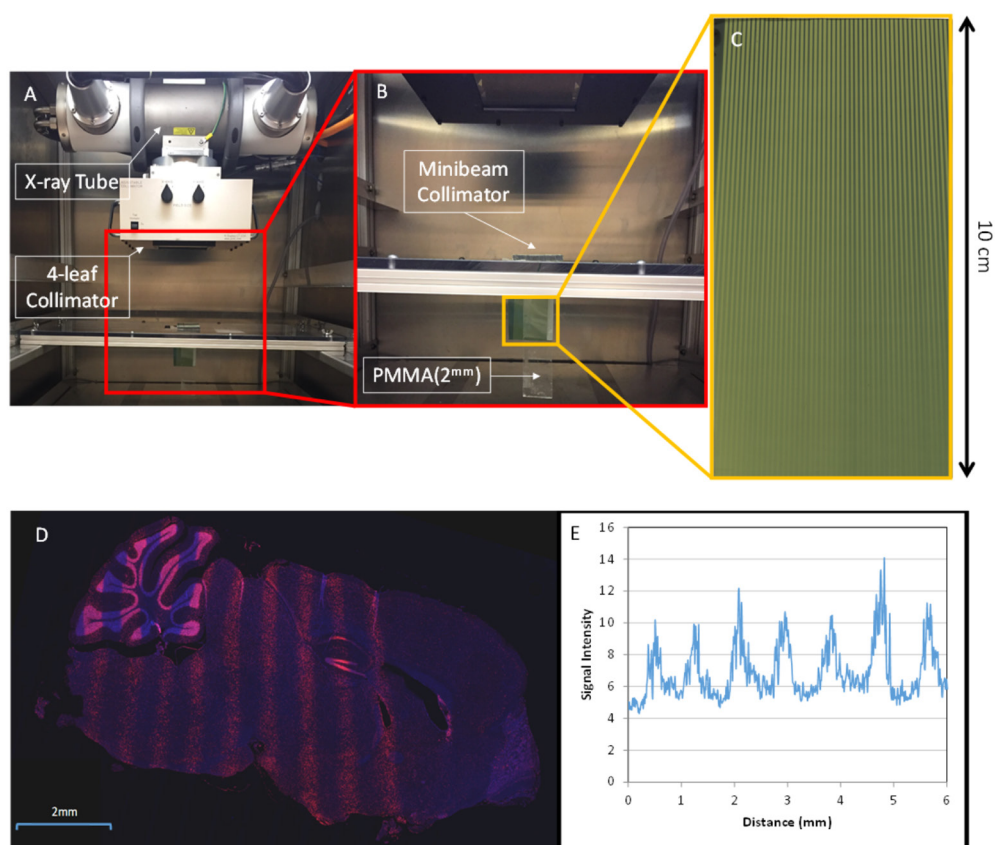


Figure 8. The spatial resolution of the MBRT in the phantom and mouse brain. A layer of EBT3 (4×10 cm) was sandwiched between two layers of PMMA (2 mm each) and placed under the minibeam collimator (the longest dimension along the beam), at 37 cm FSD (A) and (B). (C) The mini-beam behavior in the film: the peaks were distinguishable at a depth of 10 cm. (D) γ -H2AX staining of the mouse brain, 6 h post irradiation with 100 Gy MBRT: the beams kept their resolution deep in the tissue (D) and (E).

Interestingly, the tumor did not grow in one mouse that received MBRT treatment up to 60 d post tumor inoculation. As a result, MBRT was more robust in controlling the tumor growth rate than CRT (figure 10).

Discussion

Synchrotron generated micro- and minibeam radiation preclinical studies have shown promising results in sparing the normal tissue while inducing higher therapeutic effects than conventional radiation therapy (Dilmanian *et al* 2006, Deman *et al* 2012, Prezado *et al* 2015, Bouchet *et al* 2016). These findings have prompted investigators to explore ways to generate MRT and MBRT using non-synchrotron irradiators, with the goal of facilitating the translation of this promising modality to the clinic. However, most of these studies have designed complicated collimators or irradiators that confined the MRT and MBRT studies to a few labs and facilities (Babcock *et al* 2011, Hadsell *et al* 2013, Hong *et al* 2015, Bartzsch *et al* 2016). Here, we have

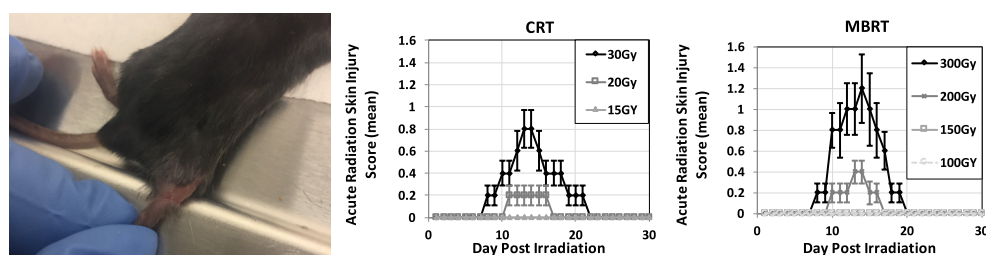


Figure 9. Normal tissue radiation injury. The image on the left demonstrates a mouse with score 3 post-irradiation acute skin injury. A mean score of acute skin injury up to 30 d post-irradiation with different CRT and MBRT_{peak} doses ($n = 5$ per group). Error bars are SE.

demonstrated a straightforward and affordable method for applying homogeneous MBRT over a large field of irradiation using an animal irradiator. Moreover, our simple method appears to be highly effective and the data generated can be reproduced in different facilities.

When compared to previous studies, the dosimetric characteristics of our method are in great agreement. The PDD pattern of peaks, valley, and PVDR is identical to previously measured and reported dosimetric evaluations of MBRT (Siegbahn *et al* 2006, Gokeri *et al* 2010, Deman *et al* 2011). The PVDR in our study is also comparable to a previously reported non-synchrotron based study (Babcock *et al* 2011). In fact, it should be noted the valley dose is generated due to Compton scatter, and consequently, it is roughly proportional to the primary peak dose from which it originates and decreases as the number of minibeam decreases (smaller radiation field size). As a result, the fact that we generated comparable PVDR while covering a larger radiation field (4 cm \times 10 cm field versus 1.75 cm circular field in the study by Babcock *et al*) and using a higher peak dose (100 Gy for peak and valley doses measurements versus 20–25 Gy in the study by Babcock *et al*) underlines the utility of our method. Furthermore, we utilized two different radiochromic films with different ranges of sensitivity to precisely measure peak and valley doses and scanned them with high resolution (1200 dpi), which enabled higher accuracy compared with previous studies (Babcock *et al* 2011). The calibration curves of EBT3 and MD-V3 in three-color channels are demonstrated in the supplemental figure 3. We also found that from ≈ 23 mm deep in the tissue, the PVDR remains almost constant within the error bars (figure 6(B)). This pattern has been reported before (Deman *et al* 2011), and illustrates the normal tissue sparing effect of this method at the exit plane. The peaks in our method dropped to 50% at lower depth compared to synchrotron generated MBRT, which was expected due to the lower mean of energy used in our experiment relative to the synchrotron (61 KeV here versus 80 KeV or higher in synchrotron studies) (Deman *et al* 2011).

The use of an industrial irradiator as the source of radiation for MRT or MBRT introduces two major limitations as shown in figure 11:

First, in MRT and MBRT, kilovolt x-ray beams are utilized in order to keep the spatial fractionation deep in the tissue. At this energy level, more than 99% of the electrons' energy would be converted to heat in the anode. In the current study, an oiled-cooled-anode irradiator with a large focal spot (8 mm) was employed that provides better heat conduction and, in addition, lessens the heel effect. So, a large homogeneous radiation field can be used to apply MRT or MBRT on a large area to minimize the duration of radiation (figure 12(A)) and consequently, lessen the chance of smearing of the beams due to physiological movements during the long radiation time. As mentioned before, we also employed minibeam instead

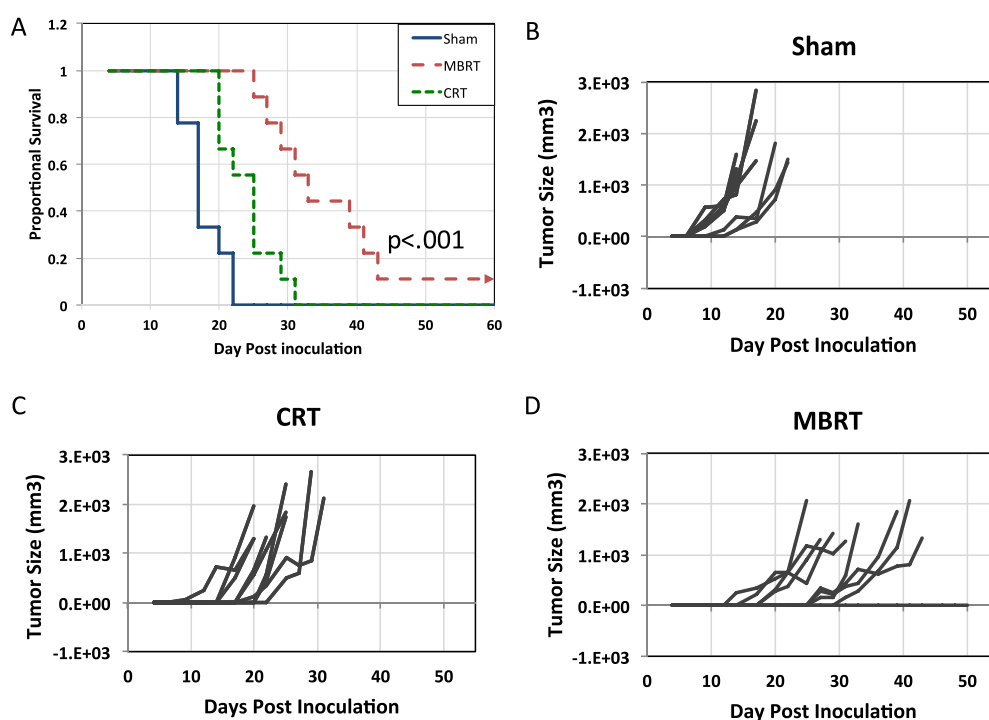


Figure 10. Mice treated for flank melanoma. Survival (A) and total tumor growth ((B)–(D)) without treatment or after either CRT or MBRT. The P -value for survival is by log-rank.

of microbeams to minimize this effect. As it is clear in figures 8(D) and (E) we were able to generate 100 Gy beams that maintained their resolution deep in the live mouse brain.

Another limitation is the fact that the industrially generated x-ray photons are divergent and, in combination with big focal size, generate a wider penumbra that increases the valley dose deep in the tissue (figure 12(B)). Several histological studies support the idea that surviving cells in the valley regions, and consequently the valley doses, play a crucial role in maintaining tissue function (Serduc *et al* 2006, Laissue *et al* 2007, Schültke *et al* 2013, Benedict *et al* 2014). As a result, a narrower penumbra is desired. We utilized the following consideration to minimize the penumbra.

1. In contrast to previous studies (Babcock *et al* 2011, Hadsell *et al* 2013b), we used a proximal collimation (the collimator was close to the target instead of the radiation source) (see figure 12(B)).
2. As shown in figure 12(C), there is an inverse relation between the penumbra and FSD. However, dose rate changes proportionally to $\left(\frac{1}{\text{FSD}^2}\right)$. Based on our previous studies (Zhang *et al* 2014a, Yuan *et al* 2015), we estimated the required dose to induce therapeutic responses with minimal effect on normal tissue to be 150–300 Gy, so to maintain the total treatment duration to less than 2 h; according to the approved protocol by IACUC to minimize animal anesthetic effects; the farthest FSD was chosen (FSD = 37 cm, dose rate = 2.9 Gy min^{-1} , collimator relative output factor = 0.84). In addition, by increasing the FSD, using a parallel-septa collimator was feasible, which eased the design and alignment of the collimator (figure 12(D)).

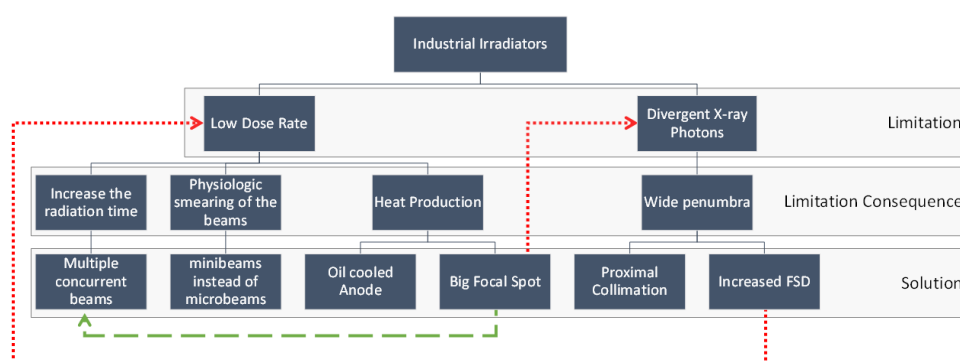


Figure 11. The major limitation in using industrial irradiators for applying MRT/MBRT and our approaches to minimize their effects. Our solution to one limitation may also help with another one (dashed line) or worsen the effect of another limitation (dotted line).

As a proof of principle, and to investigate the efficacy of our method *in vitro*, the response of two-cell lines using clonogenic assay was evaluated and the cell survival curve was generated (figure 7). This assay measures the ability of a single cell to form a colony and is based on the idea that for a tumor to be eradicated, it is only necessary to render its consisting cells unable to proliferate indefinitely (Hall and Giaccia 2012). When compared to the previously reported survival curve of these two cell lines after CRT, we found that 6 Gy of CRT will induce a comparable *in vitro* effect to almost 42 Gy of MBRT in TRP and B16-f10 (Twyman-Saint *et al* 2015, Schmid *et al* 2016). Future studies include evaluating the surviving fraction of the cells after different doses of each modality, for a precise *in vitro* comparison of the cell response to CRT versus MBRT.

Due to the distinct spatial fractionation of the x-ray beam in MRT/MBRT, finding the actual equivalent dose MRT/MBRT versus CRT is convoluted and studies have used different assumptions for the physical or biological equivalent dose. For instance, Ibahim *et al* tried to find the *in vitro* equivalent dose using clonogenic and real-time cell impedance sensing assays (Ibahim *et al* 2014). In synchrotron based MRT studies, normal tissue toxicity is more dependent on the valley region parameters because: (1) Ultra-high doses of x-ray destroy all cells along the beam path, and (2) the beam size is approximately $25\ \mu\text{m}$ – $50\ \mu\text{m}$, spaced at $200\ \mu\text{m}$ – $400\ \mu\text{m}$ on center. Consequently, most of the tissue in the radiation field receives the valley dose. In the current study, the beams to valley FWHM ratio is larger than with synchrotron microbeams, so a higher normal tissue toxicity than equivalent valley dose was expected. Since we investigated the effect on our method on SC flank tumors, the effect of different doses of MBRT and CRT on normal skin tissue *in vivo* was evaluated to find the optimal radiobiological equivalent dose (RBE). No acute skin toxicity was observed in mice that were irradiated with doses up to 150 Gy and 15 Gy in MBRT and CRT, respectively (figure 9). In a previous study, we demonstrated the sparing effect of MBRT on normal mice brain tissue post-irradiation, up to 8 months (Bazyar *et al* 2017). Currently, we are investigating the full extent of normal tissue toxicity, ED50 and TD50 of our technique on different tissues.

The *in vivo* therapeutic effect of our method was investigated using a mouse model of melanoma by applying RBE of each modality. We observed that applying MBRT using the current setting and doses was more effective in controlling the tumor growth rate than CRT ($p = 0.002$) and ablated the tumor in one out of 9 mice in MBRT group (11% chance of ablation) (figure 10). It is worth mentioning that CRT is not an effective treatment for B16-F10

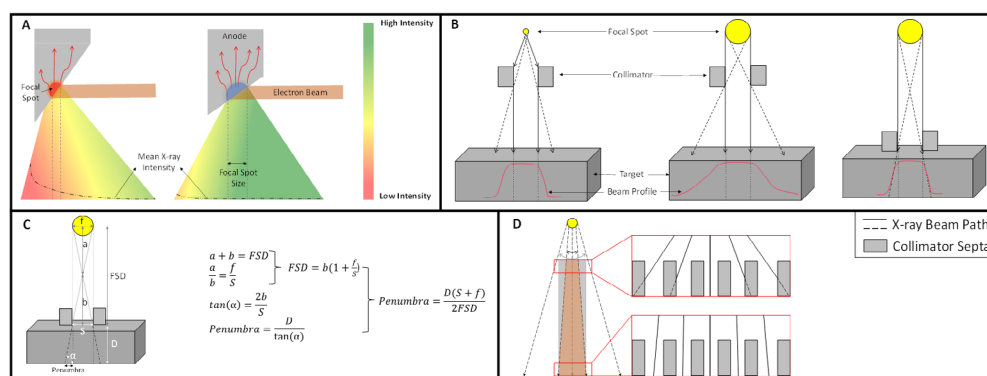


Figure 12. (A) Comparison of the generated beam intensity between a small (left) versus large (right) focal spot irradiator; (B) the comparisons in the generated beam profile deep in the tissue in the small (left) or large (middle and right) focal spot irradiator are used and the collimator is placed near the source (left and middle) versus near the target (right); (C) the equation demonstrates in large focal spot irradiators, the penumbra has an inverse relation with the focal spot to surface distance; (D) the schematic shows that by increasing the FSD, parallel septa in the collimator can be used, and a wider radiation field can be covered. The rectangle covers an equal radiation field, far or close to the source, the trapezoid area contains beams with the same degrees.

even when a higher dose (20 Gy) is applied (Twyman-Saint *et al* 2015). Several hypotheses have been postulated to explain the wider therapeutic index of MBRT/MRT:

1. The spatial fractionation pattern of MBRT/MRT provides a higher contact surface between radiated and non-irradiated tissue that increases the chance of healing.
2. MBRT/MRT may activate a different bystander response than CRT that favors the tissue healing in normal tissue and facilitates the tumor ablation (Dilmanian *et al* 2007).
3. Normal vessels demonstrate a higher resistance to MBRT/MRT than CRT, while tumor microvasculature is sensitive to MBRT/MRT (Bouchet *et al* 2015).
4. Different immune responses may be activated after MBRT/MRT than CRT (Sprung *et al* 2012).

When compared to synchrotron studies, we successfully produced a method that mimics the spatial beam pattern of synchrotron MBRT. Although in the initial MRT experiments an ultra-high dose of x-ray (up to thousands of Gys) have been utilized (Serduc *et al* 2006), recent studies demonstrated the toxicity effect appears at much lower doses (Mukumoto *et al* 2017). Serduc *et al* found that the toxicity is directly correlated to beam width (Serduc *et al* 2009). Using our approach, 150 Gy is the maximum MBRT peak dose that did not induce skin effects. Our generated beams are almost 250 μm , which are below the threshold (beamwidth $\geq 400 \mu\text{m}$) that induces a different response in normal tissue microvasculature (Brönnimann *et al* 2016). However, it should be noted that synchrotron sources may induce a different biological response due to the extremely high dose rates.

The translation of our method to clinics may encounter several technical limitations. The low dose rate and limited heat conduction capacity of clinical irradiators are the major limitations of the current method, and, consequently, developing a high intensity kilovoltage irradiator would be advantageous. Second, with proximal collimating, aligning the collimator with the source may require a greater deal of accuracy. Designing a device to mount the collimator may ease this problem. An applicator may also be needed to restrict the radiation field to the

lesion. Although normal skin demonstrated a higher resistance to MBRT in the acute phase, confining the radiation field to the lesion is always desired in order to minimize the normal tissue toxicity. Finally, beam smearing due to the long duration of therapy also remains a big consideration. One approach would be to apply MBRT by a physiologically gated irradiator (Chtcheprov *et al* 2014).

Our study has several limitations. One limitation was using radiochromic film for dosimetry. Although these films have been used extensively in MRT and MBRT studies (Crosbie *et al* 2008, Anderson *et al* 2010, Hadsell *et al* 2013, Hong *et al* 2015), currently the uncertainty levels for film dosimetry has been reported between 1% and 10% depending on the situation (Martisíková *et al* 2008, Bouchard *et al* 2009, DeWerd *et al* 2011, Palmer *et al* 2015). Here we followed the single scan, three channel protocol, recommended by the supplier to minimize errors (Efficient Protocols for Accurate Radiochromic Film Calibration and Dosimetry 2017). However, the protocol did not eliminate some reported source of errors, like film curvature at scanning (Palmer *et al* 2015). We cross-calibrated the mounted transmission chamber to an ion chamber and used the transmission plate for dose measurements. This also introduced some potential errors (1.25 ± 0.08 percentage difference between the two methods). To minimize this error, the calibration was done at a high dose (150 Gy) and checked twice. Finally, some errors were introduced from utilizing the plastic phantom (PMMA or acrylic) instead of water. Although the IAEA TRS398 code of practice approved their application for low energy x-ray dosimetry, the plastic phantom introduces error in measurements mainly due to density variation (up to 4%) in different batches, and non-homogenous thickness distribution even in one sheet (Tello *et al* 1995). The density of the sheet we used was 1.174 g cm^{-3} and we measured the entire slab and used the piece that was 2 ± 0.01 mm thick.

Conclusion

In conclusion, we have demonstrated a relatively simple and easily reproducible method for applying homogeneous MBRT using a small animal irradiator unit. We described our approach, its dosimetric characteristics, and its effectiveness *in vitro* and *in vivo*. At its current stage, our method can be used for applying MBRT in preclinical studies.

Acknowledgments

We wish to thank the UNC Translational Pathology Laboratory (TPL) staff for their help in preparing, scanning, and interpretation of the histology slides. We also thank Dr C Ryan Miller and Robert S McNeil at UNC Translational Neuro-oncology Laboratory for their generous help and guidance with the Clonogenic Assay of the cells. The authors also appreciate the efforts of the Physics Shop and Makerspace staff at UNC-CH for making the mouse holder and shielding platform.

ORCID iDs

Soha Bazyar  <https://orcid.org/0000-0002-8425-8281>

Christina R Inscoc  <https://orcid.org/0000-0001-8681-9030>

Yueh Z Lee  <https://orcid.org/0000-0003-1846-7680>

References

- Anderson D, Warkentin B, Siegbahn E A and Fallone B G 2010 Sci-Fri PM: delivery-01: dosimetry for microbeam radiation therapy at the canadian light source *Med. Phys.* **37** 3904
- Armoogum K and Thorp N 2015 Dosimetric comparison and potential for improved clinical outcomes of paediatric CNS patients treated with protons or IMRT *Cancers* **7** 706–22
- Babcock K, Sidhu N, Kundapur V and Ali K 2011 Collimator design for experimental minibeam radiation therapy *Med. Phys.* **38** 2192–7
- Bartzsch S, Cummings C, Eismann S and Oelfke U 2016 A preclinical microbeam facility with a conventional x-ray tube *Med. Phys.* **43** 6301
- Bazyar S, Inscoe C R, Benefield T, Zhang L, Lu J, Zhou O and Lee Y Z 2017 Neurocognitive sparing of desktop microbeam irradiation *Radiat. Oncol.* **12** 127
- Benedict S H, Schlesinger D J, Goetsch S J and Kavanagh B D 2014 *Stereotactic Radiosurgery and Stereotactic Body Radiation Therapy* (Boca Raton, FL: CRC Press)
- Bouchard H, Lacroix F, Beaudoin G, Carrier J-F and Kawrakow I 2009 On the characterization and uncertainty analysis of radiochromic film dosimetry *Med. Phys.* **36** 1931–46
- Bouchet A, Bräuer-Krisch E, Prezado Y, El Atifi M, Rogalev L, Le Clec'h C, Laissue J A, Pelletier L and Le Duc G 2016 Better efficacy of synchrotron spatially microfractionated radiation therapy than uniform radiation therapy on glioma *Int. J. Radiat. Oncol. Biol. Phys.* **95** 1485–94
- Bouchet A, Serduc R, Laissue J A and Djonov V 2015 Effects of microbeam radiation therapy on normal and tumoral blood vessels *Phys. Med.* **31** 634–41
- Brönnimann D, Bouchet A, Schneider C, Potez M, Serduc R, Bräuer-Krisch E, Graber W, von Gunten S, Laissue J A and Djonov V 2016 Synchrotron microbeam irradiation induces neutrophil infiltration, thrombocyte attachment and selective vascular damage *in vivo Sci. Rep.* **6** 33601
- Casanova Borca V, Pasquino M, Russo G, Grosso P, Cante D, Sciacero P, Girelli G, La Porta M R and Tofani S 2013 Dosimetric characterization and use of GAFCHROMIC EBT3 film for IMRT dose verification *J. Appl. Clin. Med. Phys.* **14** 4111
- Chtcheprov P, Burk L, Yuan H, Inscoe C, Ger R, Hadsell M, Lu J, Zhang L, Chang S and Zhou O 2014 Physiologically gated microbeam radiation using a field emission x-ray source array *Med. Phys.* **41** 081705
- Crosbie J C, Svalbe I, Midgley S M, Yagi N, Rogers P A W and Lewis R A 2008 A method of dosimetry for synchrotron microbeam radiation therapy using radiochromic films of different sensitivity *Phys. Med. Biol.* **53** 6861–77
- Deman P, Vautrin M, Stupar V, Barbier E L, Elleaume H, Esteve F and Adam J F 2011 Monochromatic minibeam radiotherapy: theoretical and experimental dosimetry for preclinical treatment plans *Phys. Med. Biol.* **56** 4465–80
- Deman P et al 2012 Monochromatic minibeam radiotherapy: from healthy tissue-sparing effect studies toward first experimental glioma bearing rats therapy *Int. J. Radiat. Oncol. Biol. Phys.* **82** e693–700
- DeWerd L A, Ibbott G S, Meigooni A S, Mitch M G, Rivard M J, Stump K E, Thomadsen B R and Venselaar J L M 2011 A dosimetric uncertainty analysis for photon-emitting brachytherapy sources: report of AAPM task group no. 138 and GEC-ESTRO *Med. Phys.* **38** 782–801
- Dilmanian F A, Morris G M, Zhong N, Bacarian T, Hainfeld J F, Kalef-Ezra J, Brewington L J, Tammam J and Rosen E M 2003 Murine EMT-6 carcinoma: high therapeutic efficacy of microbeam radiation therapy *Radiat. Res.* **159** 632–41
- Dilmanian F A, Qu Y, Feinendegen L E, Peña L A, Bacarian T, Henn F A, Kalef-Ezra J, Liu S, Zhong Z and McDonald J W 2007 Tissue-sparing effect of x-ray microplanar beams particularly in the CNS: is a bystander effect involved? *Exp. Hematol.* **35** 69–77
- Dilmanian F A, Zhong Z, Bacarian T, Benveniste H, Romanelli P, Wang R, Welwart J, Yuasa T, Rosen E M and Anselm D J 2006 Interlaced x-ray microplanar beams: a radiosurgery approach with clinical potential *Proc. Natl Acad. Sci. USA* **103** 9709–14
- Efficient Protocols for Accurate Radiochromic Film Calibration and Dosimetry 2017 Available at: www.gafchromic.com/documents/Efficient%20Protocols%20for%20Calibration%20and%20Dosimetry.pdf (Accessed: 26 October 2017)
- Franken N A P, Rodermond H M, Stap J, Haveman J and van Bree C 2006 Clonogenic assay of cells *in vitro Nat. Protoc.* **1** 2315–9
- Gafchromic™ dosimetry media, type EBT-3 2017 Available at: www.gafchromic.com/documents/EBT3_Specifications.pdf (Accessed: 26 October 2017)

- Gafchromic[®] Dosimetry Media, Type MD-V3 2017 Available at: www.peo-radiation-technology.com/wp-content/uploads/2015/08/ash_15_gafchromic_hd-v3_datasheet_peo.pdf (Accessed: 26 October 2017)
- Gafchromic[™] Dosimetry Tools, Design for a Contemporary RT Environment 2017 Available at: www.gafchromic.com/documents/PC-11802_Gafchromic_EBT3.pdf (Accessed: 26 October 2017)
- Gokeri G, Kocar C and Tombakoglu M 2010 Monte Carlo simulation of microbeam radiation therapy with an interlaced irradiation geometry and an Au contrast agent in a realistic head phantom *Phys. Med. Biol.* **55** 7469–87
- Hadsell J M J 2013a The development and characterization of a first generation carbon nanotube x-ray based microbeam radiation therapy system *Doctoral Dissertation* The University of North Carolina at Chapel Hill
- Hadsell M *et al* 2013b A first generation compact microbeam radiation therapy system based on carbon nanotube x-ray technology *Appl. Phys. Lett.* **103** 183505
- Hall E J and Giaccia A J 2012 *Radiobiology for the Radiologist* (Baltimore, MD: Williams and Wilkins)
- Hendry J H, Jeremic B and Zubizarreta E H 2006 Normal tissue complications after radiation therapy *Rev. Panam. Salud Publica* **20** 2–3
- Hong Z, Zenkoh J, Le B, Gerelchuluun A, Suzuki K, Moritake T, Washio M, Urakawa J and Tsuboi K 2015 Generation of low-flux x-ray micro-planar beams and their biological effect on a murine subcutaneous tumor model *J. Radiat. Res.* **56** 768–76
- Ibahim M J, Crosbie J C, Yang Y, Zaitseva M, Stevenson A W, Rogers P A W and Paiva P 2014 An evaluation of dose equivalence between synchrotron microbeam radiation therapy and conventional broadbeam radiation using clonogenic and cell impedance assays *PLoS One* **9** e100547
- Laisue J A, Blattmann H, Wagner H P, Grotzer M A and Slatkin D N 2007 Prospects for microbeam radiation therapy of brain tumours in children to reduce neurological sequelae *Dev. Med. Child Neurol.* **49** 577–81
- Ma C-M, Coffey C W, DeWerd L A, Liu C, Nath R, Seltzer S M and Seuntjens J P 2001 AAPM protocol for 40–300kV x-ray beam dosimetry in radiotherapy and radiobiology *Med. Phys.* **28** 868–93
- Martisíková M, Ackermann B and Jäkel O 2008 Analysis of uncertainties in Gafchromic EBT film dosimetry of photon beams *Phys. Med. Biol.* **53** 7013–27
- Mukumoto N *et al* 2017 Sparing of tissue by using micro-slit-beam radiation therapy reduces neurotoxicity compared with broad-beam radiation therapy *J. Radiat. Res.* **58** 17–23
- Nolan M W, Gieger T L, Karakashian A A, Nikolova-Karakashian M N, Posner L P, Roback D M, Rivera J N and Chang S 2017 Outcomes of spatially fractionated radiotherapy (GRID) for bulky soft tissue sarcomas in a large animal model *Technol. Cancer Res. Treat.* **16** 357–65
- Overwijk W W and Restifo N P 2001 B16 as a mouse model for human melanoma *Curr. Protoc. Immunol.* ch 20 Unit 20 (<https://doi.org/10.1002/0471142735.im2001s39>)
- Palmer A L, Bradley D A and Nisbet A 2015 Evaluation and mitigation of potential errors in radiochromic film dosimetry due to film curvature at scanning *J. Appl. Clin. Med. Phys.* **16** 5141
- Poludniowski G G 2007 Calculation of x-ray spectra emerging from an x-ray tube. Part II. X-ray production and filtration in x-ray targets *Med. Phys.* **34** 2175–86
- Poludniowski G G and Evans P M 2007 Calculation of x-ray spectra emerging from an x-ray tube. Part I. Electron penetration characteristics in x-ray targets *Med. Phys.* **34** 2164–74
- Poludniowski G, Landry G, DeBlois F, Evans P M and Verhaegen F 2009 SpekCalc: a program to calculate photon spectra from tungsten anode x-ray tubes *Phys. Med. Biol.* **54** N433–8
- Pommier P, Gomez F, Sunyach M P, D’Hombres A, Carrie C and Montbarbon X 2004 Phase III randomized trial of Calendula officinalis compared with trolamine for the prevention of acute dermatitis during irradiation for breast cancer *J. Clin. Oncol.* **22** 1447–53
- Prezado Y, Deman P, Varlet P, Jouvion G, Gil S, Le Clec’H C, Bernard H, Le Duc G and Sarun S 2015 Tolerance to dose escalation in minibeam radiation therapy applied to normal rat brain: long-term clinical, radiological and histopathological analysis *Radiat. Res.* **184** 314–21
- Schmid R S *et al* 2016 Core pathway mutations induce de-differentiation of murine astrocytes into glioblastoma stem cells that are sensitive to radiation but resistant to temozolomide *Neuro Oncol.* **18** 962–73
- Schültke E, Trippel M, Bräuer-Krisch E, Renier M, Bartzsch S, Requardt H, Döbrössy M D and Nikkhah G 2013 Pencilbeam irradiation technique for whole brain radiotherapy: technical and biological challenges in a small animal model *PLoS One* **8** e54960
- Serduc R *et al* 2009 Synchrotron microbeam radiation therapy for rat brain tumor palliation-influence of the microbeam width at constant valley dose *Phys. Med. Biol.* **54** 6711–24

- Serduc R *et al* 2006 *In vivo* two-photon microscopy study of short-term effects of microbeam irradiation on normal mouse brain microvasculature *Int. J. Radiat. Oncol. Biol. Phys.* **64** 1519–27
- Siegbahn E A, Stepanek J, Bräuer-Krisch E and Bravin A 2006 Determination of dosimetric quantities used in microbeam radiation therapy (MRT) with Monte Carlo simulations *Med. Phys.* **33** 3248–59
- Smyth L M L, Senthil S, Crosbie J C and Rogers P A W 2016 The normal tissue effects of microbeam radiotherapy: what do we know, and what do we need to know to plan a human clinical trial? *Int. J. Radiat. Biol.* **92** 302–11
- Sprung C N, Yang Y, Forrester H B, Li J, Zaitseva M, Cann L, Restall T, Anderson R L, Crosbie J C and Rogers P A W 2012 Genome-wide transcription responses to synchrotron microbeam radiotherapy *Radiat. Res.* **178** 249–59
- Tello V M, Taylor R C and Hanson W F 1995 How water equivalent are water-equivalent solid materials for output calibration of photon and electron beams? *Med. Phys.* **22** 1177–89
- Twyman-Saint V C *et al* 2015 Radiation and dual checkpoint blockade activate non-redundant immune mechanisms in cancer *Nature* **520** 373–7
- Xtrahl 200 and 300 2017 Available at: www.radiustech.it/upld/catalogo/doc/Xstrahl_Medical_200_300_LR.pdf (Accessed: 26 October 2017)
- Yuan H, Zhang L, Frank J E, Inscoc C R, Burk L M, Hadsell M, Lee Y Z, Lu J, Chang S and Zhou O 2015 Treating brain tumor with microbeam radiation generated by a compact carbon-nanotube-based irradiator: initial radiation efficacy study *Radiat. Res.* **184** 322–33
- Zhang L, Yuan H, Burk L M, Inscoc C R, Hadsell M J, Chtcheprov P, Lee Y Z, Lu J, Chang S and Zhou O 2014a Image-guided microbeam irradiation to brain tumour bearing mice using a carbon nanotube x-ray source array *Phys. Med. Biol.* **59** 1283–303
- Zhang L, Yuan H, Inscoc C R, Chtcheprov P, Hadsell M, Lee Y Z, Lu J, Chang S and Zhou O 2014b Nanotube x-ray for cancer therapy: a compact microbeam radiation therapy system for brain tumor treatment *Expert Rev. Anticancer Ther.* **14** 1411–8